Electronic Supplementary Material

RuO_2 clusters derived from bulk $SrRuO_3$: Robust catalyst for oxygen evolution reaction in acid

Muwei Ji[1,2,§], Xin Yang[3,§], Shengding Chang[3,§], Wenxing Chen[4,§], Jin Wang[1,3,§] (✉), Dongsheng He[5],Yao Hu[3], Qian Deng[3], You Sun[3], Bo Li[3], Jingyu Xi[3], Tomoaki Yamada[6], Jiatao Zhang[4], Hai Xiao[7], Caizhen Zhu[2], Jia Li[3] (✉), and Yadong Li[7] (✉)

[1] *College of Materials Science and Engineering, Shenzhen University, Shenzhen 518060, China*
[2.] *Institute of Low-Dimensional Materials Genome Initiative, College of Chemistry and Environmental Engineering of Shenzhen University, Shenzhen 518060, China*
[3.] *Tsinghua Shenzhen International Graduate School, Tsinghua University, Shenzhen 518055, China*
[4.] *Beijing Key Laboratory of Construction Tailorable Advanced Functional Materials and Green Applications, School of Materials Science and Engineering, Beijing Institute of Technology, Beijing 100081, China*
[5.] *Materials Characterization and Preparation Center, Southern University of Science and Technology, Shenzhen 518055, China*
[6.] *Department of Energy Engineering, Nagoya University, Furo-cho, Chikusa-ku, Nagoya 464-8603, Japan*
[7.] *Department of Chemistry, Tsinghua University, Beijing 100084, China*
[§] *Muwei Ji, Xin Yang, Shengding Chang, Wenxing Chen and Jin Wang contributed equally to this work.*

Supporting information to https://doi.org/10.1007/s12274-021-3843-8

Supplemental Methods:

s1. Preparation of $SrRuO_3$ film on $SrTiO_3$ substrate:

The epitaxial $SrRuO_3$ films were deposited on (100)-$SrTiO_3$ substrate by pulsed laser deposition (PLD) technique at 700°C and 200 mTorr O_2. The thickness of the $SrRuO_3$ film is about 50 nm with the XRD diffraction pattern shown in **Figure S4**. The $SrRuO_3$ (200) peak has the Laue oscillations, which indicates the flat interface and surface of the film.

S2. Conductivity characterization of $SrRuO_3$ ceramic electrode:

The conductivity experiment was carried out by using an electrochemical workstation CHI760E and the $SrRuO_3$ was pasted on the Pt disk and then was taken as working electrode (WE). A Pt plate (1×1 cm^2) was taken as reference Electrode (RE) and count electrode (CE) (Figure I). The current-voltage (I-V) curve was collected by using linear sweep voltammetry (LSV) methods with the scanning window was set from -60 to 60 mV at a scanning rate of 10 $mV \cdot s^{-1}$.

S3. Structural characterization:

The X-ray diffraction (XRD) patterns of samples were obtained with Bruker D8 X-ray diffractometer with Cu Kα radiation (λ = 1.5418 Å). The surface morphology was characterized on ZEISS SUPRA® 55 scanning electron microscope (SEM). High resolution transmission electron microscopy (HRTEM) study was carried out on Tecnai G2 F30 equipped with an EDX detector (Oxford X-Max 20). High-angle annular dark-field scanning transmission electron (HAADF-STEM) images were collected by using Titan Cubed Themis G2 300 operating at 300 KV. X-ray photoelectron spectroscopy (XPS) was performed on PHI-5000 VersaprobeII(Ulvac-Phi, Japan). The specific surface area of as-prepared RuO_2 clusters was measured with BET analyzer (BELSORP-Max).

Address correspondence to Jin Wang, wangjin19@szu.edu.cn; Jia Li, li.jia@sz.tsinghua.edu.cn; Yadong Li, ydli@tsinghua.edu.cn

S4. Sr and Ru corrosion measured by inductively coupled plasma- atom emission absorption spectra:

Sr and Ru corroded from the working electrode during OER test were measured by inductively coupled plasma-atomic emission spectrometer (JY2000-2, HORIBA JOBINYVON).

S5. Synchrotron characterization:

The X-ray absorption fine structure spectra (Ru K-edge) were collected at BL14W1 station in Shanghai Synchrotron Radiation Facility (SSRF, the storage ring was operated at 3.5 GeV with a maximum current of 250 mA). The data were collected at room temperature in transmission mode using N_2-filled ionization chamber (Si (311) monochromator for Ru K-edge). All samples were pelletized as disks of 13 mm diameter using graphite powder as a binder (ground thoroughly by mortar and pestle).

The acquired EXAFS data were processed according to the standard procedures using the ATHENA module implemented in the IFEFFIT software packages. The k^2-weighted EXAFS spectra were obtained by subtracting the post-edge background from the overall absorption and then normalizing with respect to the edge-jump step. Subsequently, k^2-weighted $\chi(k)$ data of Ru K-edge were Fourier transformed to real (R) space using a hanning windows (dk=1.0 $Å^{-1}$) to separate the EXAFS contributions from different coordination shells. To obtain the quantitative structural parameters around central atoms, least-squares curve parameter fitting was performed using the ARTEMIS module of IFEFFIT software packages.

The following EXAFS equation was used:

$$\chi(k) = \sum_j \frac{N_j S_0^2 F_j(k)}{k R_j^2} \exp[-2k^2\sigma_j^2] \exp[\frac{-2R_j}{\lambda(k)}] \sin[2kR_j + \phi_j(k)]$$

S_0^2 is the amplitude reduction factor, $F_j(k)$ is the effective curved-wave backscattering amplitude, N_j is the number of neighbors in the j^{th} atomic shell, R_j is the distance between the X-ray absorbing central atom and the atoms in the j^{th} atomic shell (backscatterer), λ is the mean free path in Å, $\phi_j(k)$ is the phase shift (including the phase shift for each shell and the total central atom phase shift), σ_j is the Debye-Waller parameter of the j^{th} atomic shell (variation of distances around the average R_j). The functions $F_j(k)$, λ and $\phi_j(k)$ were calculated with the ab initio code FEFF8.2. The additional details for EXAFS simulations are given below.

S6. DFT Simulation:

All spin-polarized calculations are performed within the framework of density functional theory, as implemented in Vienna ab initio Simulation Package (VASP) code.[1, 2] The projected augmented wave (PAW) pseudopotential[3] is employed to describe the electron-ion interaction, and the kinetic energy cutoff is adopted as 520 eV after strict convergence tests. The exchange-correlation energy is described by using the Perdew-Burke-Ernzerhof (PBE) functional within generalized gradient approximation (GGA).[4] The van del Waals functional rvv10 is employed for the inclusion of the ubiquitous long-range interaction.[5, 6] A 4×5×1 gamma centered sampling of *k*-points in reciprocal space is used for 3×1 supercell of the four-layer RuO_2 (110) slab. Considering the solvent effect, an explicit solvation scheme is introduced in our calculations[7].

Figures S1-S15:

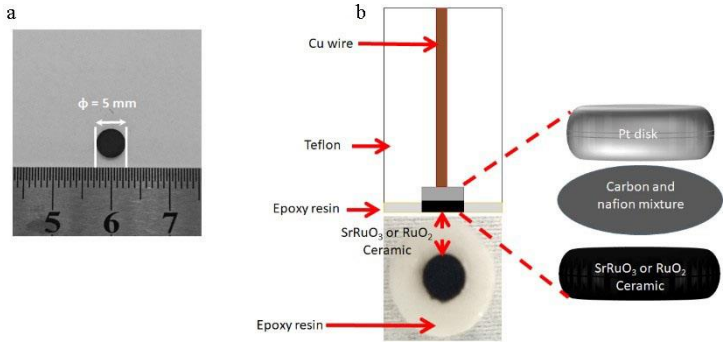

Figure S1 (a) The photograph of as-prepared $SrRuO_3$ ceramic plate with 5 mm of diameter, which was employed as electrode for preparing RuO_2 clusters. **(b)** The illustration of fabricating $SrRuO_3$ electrode.

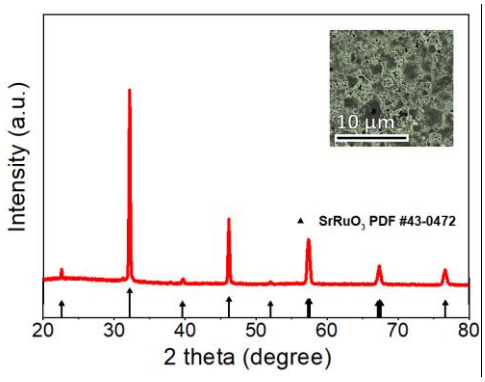

Figure S2 XRD pattern of as-prepared $SrRuO_3$ ceramic electrodes. The inset is the SEM image

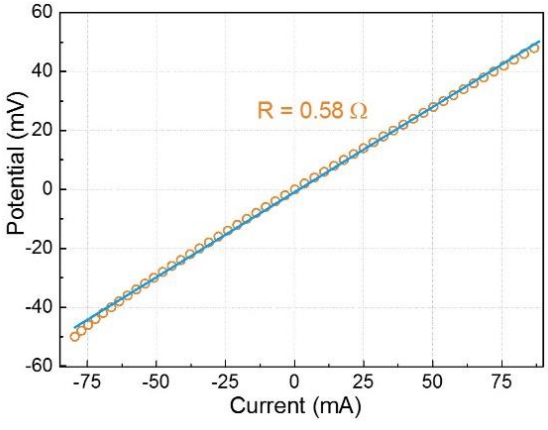

Figure S3 The current-voltage (*I-V*) characteristic of as-prepared $SrRuO_3$ ceramic electrode. The resistance of $SrRuO_3$ ceramic is measured as 0.58 ohm which reveals the good Ohmic contact at the $SrRuO_3$/Pt-disk-electrode interface.

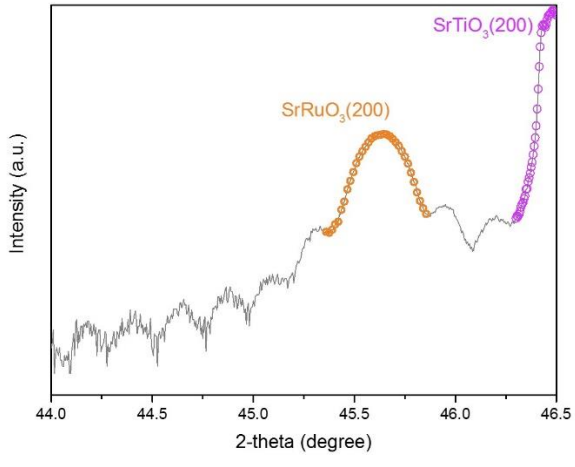

Figure S4 The XRD pattern of $SrRuO_3$ film epitaxially grown on (100)-$SrTiO_3$ substrate. The peak around 45.6 degree is assigned to $SrRuO_3$ (200) (orange circles) while the peak around 46.5 degree is to $SrTiO_3$ (200).

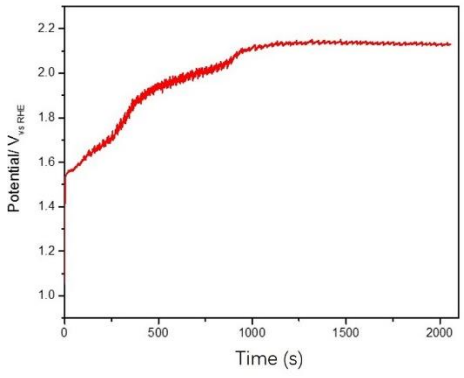

Figure S5 The chronopotentiometry (CP) curve of $SrRuO_3$ film epitaxially grown on (100)-$SrTiO_3$ substrate in 1.0 M $HClO_4$ solution at 10 mA·cm^{-2} current density. The potential rises up quickly and reaches 2.10 V (vs. RHE) within 1000 seconds.

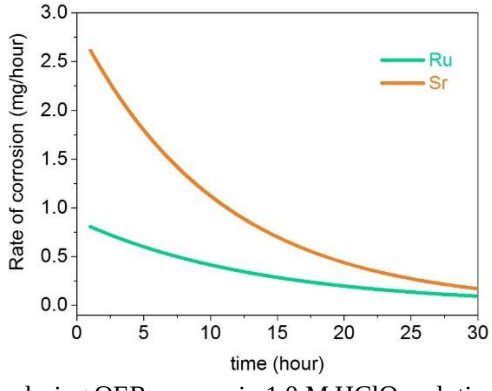

Figure S6 The leaching rate of Sr and Ru during OER process in 1.0 M $HClO_4$ solution, showing that Sr leaches more rapidly than Ru. The plots are derived from the differential of leached Sr and Ru (inset of Figure 1b) with respect to time.

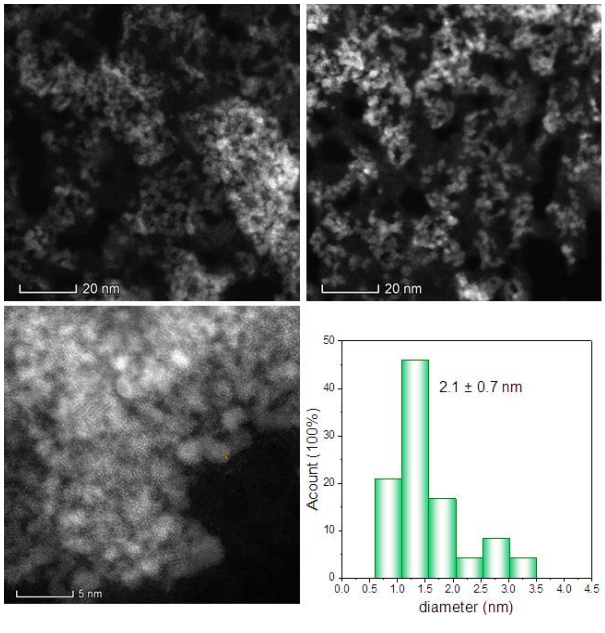

Figure S7 The STEM image of RuO_2 clusters in large scale and their size distribution.

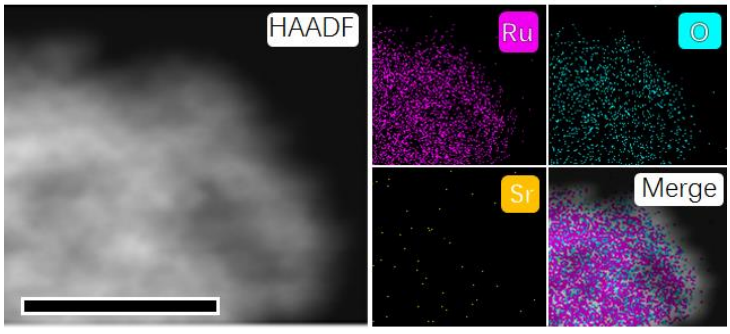

Figure S8 The STEM images and element mapping of as-prepared RuO_2 clusters. Scale bar, 1 μm. The element analysis confirmed absence of Sr in the as-prepared clusters.

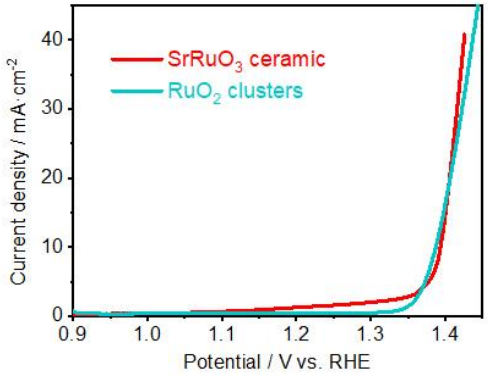

Figure S9 The OER polarization curves of $SrRuO_3$ ceramic and RuO_2 clusters.

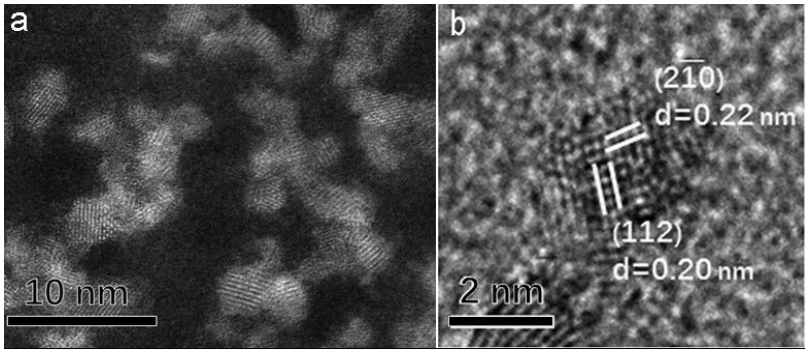

Figure S10 The TEM characterization of RuO_2 clusters after 30-hour CP measurement: (a) STEM image of RuO_2 clusters, (b) HRTEM image of which the lattice fringes can be indexed to a rutile RuO_2 phase. The TEM analysis post catalysis illustrates that the RuO_2 clusters were stable during OER catalysis.

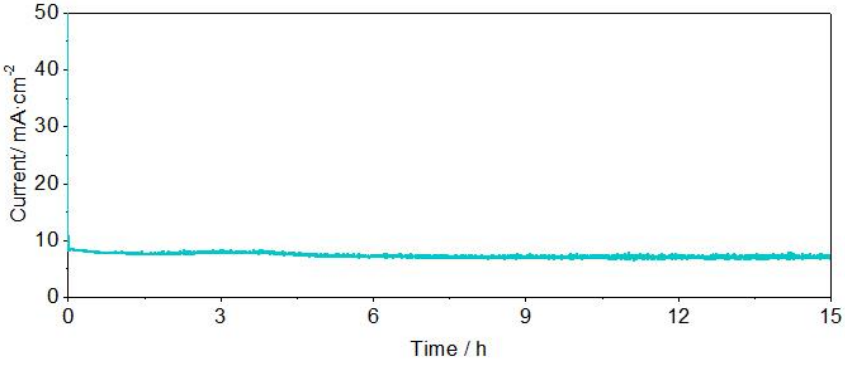

Figure S11 The CA curve of RuO_2 cluster under 1.39 V_{RHE} of potential.

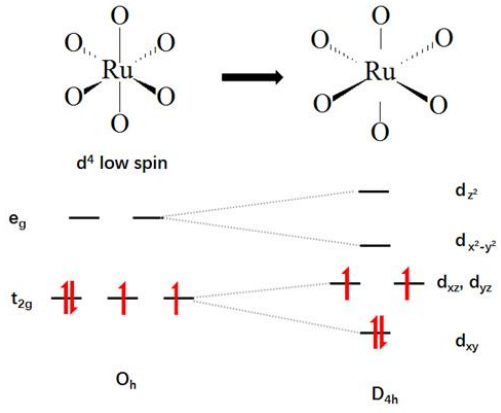

Figure S12 Illustration of *d* electron distribution of RuO_2 without (left) and with (right) Jahn-Teller effect.

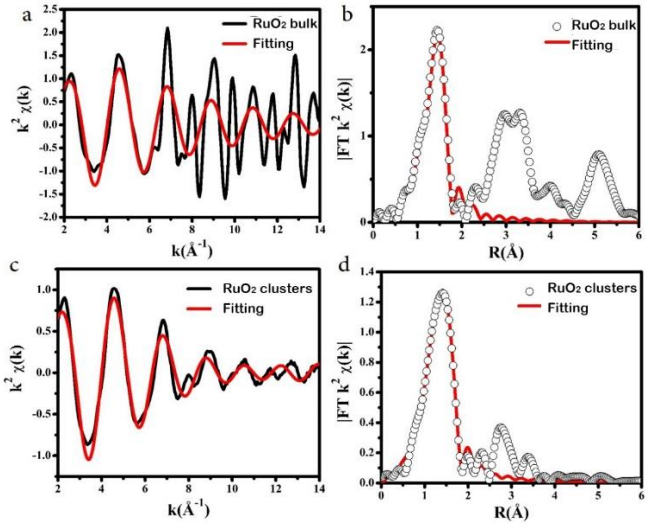

Figure S13 The k^2-weighted $\chi(k)$ data of Ru K-edge fitting plots (a-b): RuO_2 bulk and (c-d): RuO_2 clusters.

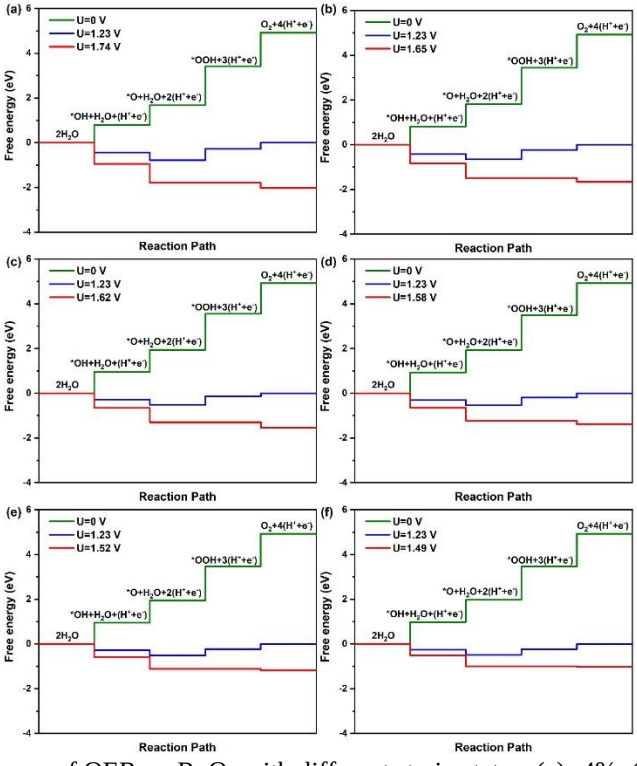

Figure S14 The free energy diagram of OER on RuO_2 with different strain states: (a) -4%; (b) 2%; (c) 0; (d) 2%; (e) 4%; (f) 6%. The green, blue and red lines indicate the reaction path under 0 V, 1.23 V and equilibrium potential.

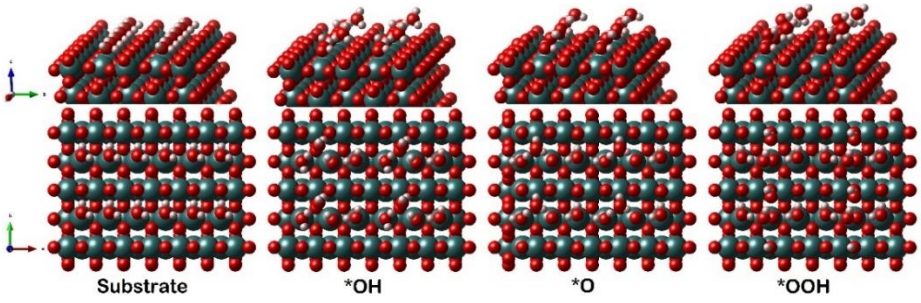

Figure S15 The employed atomic model in the DFT study, where green, red and white circles represent Ru, O and H atoms respectively.

Tables S1-S8:

Table S1 ICP results of the electrolyte solution after 30-hour OER test of $SrRuO_3$ ceramic electrode and 4.0 mg·cm^{-2}-loaded RuO_2-cluster electrode (both with 0.2 cm^2 geometric area).

	$SrRuO_3$ ceramic		**RuO_2 clusters**	
Elements in electrolyte/ppm	Ru	Sr	Ru	Sr
	27.8	75.8	1.035	N.D.

N. D. stands for the concentration lower than the detection limit (0.005ppm)

Table S2 List of overpotential at 50 mA·mg^{-1} mass current density.

Materials	**Electrolyte**	**Over-potential / mV @ 50mA·mg^{-1}**	**Loading mass/ mg·cm^{-2}**	**Reference**
RuO_2 in this work	1.0 M $HClO_4$	190	0.5	-
1D-RuO_2-CNx	0.5 M H_2SO_4	≈ 250	0.17	ACS Appl. Mater. Interfaces 2016, 8, 28678
C-RuO_2	0.5 M H_2SO_4	≈ 420	0.17	ACS Appl. Mater. Interfaces 2016, 8, 28678
IrO_2	1.0 M H_2SO_4	≈ 320	0.25	Adv. Funct. Mater. 2018, 28, 1704796.
$Ru_{0.8}Ir_{0.2}O_2$	0.5 M H_2SO_4	≈ 445	0.38	Appl. Cat B: Environmental 111–112 (2012) 376– 380.
IrO_2·RuO_2@Ru(1:1)	0.5 M H_2SO_4	≈ 320	0.379	J. Mater. Chem. A, 2017, 5, 17221.
IrO_2@MnO_2	0.1 M $HClO_4$	≈280	0.2	ACS Appl. Mater. Interfaces 2017, 9, 41855.

Table S3 The specific current of as-prepared RuO_2 clusters at 1.4 V vs. RHE and 1.5 V vs. RHE respectively in comparison with the reported values in literature.

Materials	**Electrolyte**	***Specific i* (μA·cm^{-2}) *i* @1.4 V vs RHE**	**Ref.**
RuO_2 clusters	1 M $HClO_4$	10.12 ± 2.61	In this work
RuO_2 coated on Ti foil	1 M H_2SO_4	0.24	J. Chem. Soc. Faraday Trans. 1977, 73, 1659.
RuO_2	1 M $HClO_4$	0.46	Electrochim. Acta 2011, 56, 5, 2009.
RuO_2 NPs	1 M $HClO_4$	< 0.01	J. Phys. Chem. Lett. 2012, 3, 399.

Table S4 Jahn-Teller effect for various *d* electron configurations [1].

Number of d electrons	1	2	3	4		5		6		7		8	9	10
High/Low spin				HS	LS	HS	LS	HS	LS	HS	LS			
Strength of Jahn-Teller effect	w	w	n	s	w	n	w	w	n	w	s	n	s	n

Where HS is high spin, LS is low spin, w is weak Jahn–Teller effect (t_{2g} orbitals unevenly occupied), s is strong Jahn–Teller effect expected (e_g orbitals unevenly occupied) and n is no Jahn–Teller effect expected.

Table S5 Structural parameters extracted from the Ru K-edge EXAFS fitting (S_{02}=0.85).

sample	Scattering pair	R(Å)	$\sigma^2(10^{-3}Å^2)$	ΔE_0(eV)	R factor
RuO_2 clusters	Ru-Ov	1.89	4.3	-4.2	0.001
	Ru-Op	2.02	5.6		
RuO_2 bulk	Ru-Ov	1.88	5.0	-3.2	0.004
	Ru-Op	1.99	3.8		

R is interatomic distance (the bond length between central atoms and surrounding coordination atoms); σ^2 is Debye-Waller factor (a measure of thermal and static disorder in absorber-scatterer distances); ΔE_0 is edge-energy shift (the difference between the zero kinetic energy value of the sample and that of the theoretical model). R factor is used to value the goodness of the fitting.

Error bounds that characterize the structural parameters obtained by EXAFS spectroscopy were estimated as R ± 1%; σ^2 ± 20%; ΔE_0 ± 20%.

RuO_2 bulk (FT range: 2.0-12.4 $Å^{-1}$; fitting range: 0.5-2.1 Å)

RuO_2 clusters (FT range: 2.0-12.4 $Å^{-1}$; fitting range: 0.5-2.1 Å)

Table S6 ZPE and entropic corrections at T = 298.15 K. Taken from Man *et al*' s study[8].

	*OH	*O	*OOH	H_2O	H_2
ZPE	0.36	0.07	0.40	0.56	0.27
TS	~	~	~	0.67	0.41

Table S7 Binding energies of *OH, *O and *OOH on RuO_2 (110) slab.

Strain	ΔE_{*OH}	ΔE_{*O}	ΔE_{*OOH}
-4%	0.398	1.642	3.010
-2%	0.410	1.765	3.040
0	0.554	1.899	3.145
2%	0.534	1.881	3.087
4%	0.545	1.903	3.057
6%	0.580	1.934	3.051

Table S8 The geometrical parameters and computational band center.

Strain	Surface Ru-Op (Å)	Surface Ru-Ov (Å)	Overpotential (V)	*d* center (eV)	*dxz,yz* center (eV)
-4%	1.933	1.864	0.508	-2.022	-1.865
-2%	1.948	1.869	0.415	-1.910	-1.780
0	1.965	1.869	0.386	-1.802	-1.700
2%	1.984	1.867	0.347	-1.716	-1.639
4%	2.005	1.866	0.294	-1.633	-1.579
6%	2.026	1.864	0.257	-1.571	-1.536

References

1. Kresse, G.; Furthmuller, J., Efficiency of ab-initio total energy calculations for metals and semiconductors using a plane-wave basis set. *Computational Materials Science* **1996,** *6* (1), 15-50.
2. Kresse, G.; Furthmuller, J., Efficient iterative schemes for ab initio total-energy calculations using a plane-wave basis set. *Physical Review B* **1996,** *54* (16), 11169-11186.
3. Kresse, G.; Joubert, D., From ultrasoft pseudopotentials to the projector augmented-wave method. *Physical Review B* **1999,** *59* (3), 1758-1775.
4. Perdew, J. P.; Burke, K.; Ernzerhof, M., Generalized gradient approximation made simple. *Physical Review Letters* **1996,** *77* (18), 3865-3868.
5. Vydrov, O. A.; Van Voorhis, T., Nonlocal van der Waals density functional: the simpler the better. *the Journal of Chemical Physics* **2010,** *133* (24), 244103.
6. Sabatini, R.; Gorni, T.; de Gironcoli, S., Nonlocal van der Waals density functional made simple and efficient. *Physical Review B* **2013,** *87* (4), 041108.
7. Shriver, D. F.; Atkins, P. W. (1999). *Inorganic Chemistry* (3rd ed.). Oxford University Press. pp. 235–236. ISBN 978-0-19-850330-9.
8. Briquet, L. G. V.; Sarwar, M.; Mugo, J.; Jones, G.; Calle-Vallejo, F., A New Type of Scaling Relations to Assess the Accuracy of Computational Predictions of Catalytic Activities Applied to the Oxygen Evolution Reaction. *ChemCatChem* **2017,** *9* (7), 1261-1268.
9. I. C. Man, H-Y. Su, F. Calle-Vallejo, H. A. Hansen, J. I. Martinez,N. G. Inoglu, J. Kitchin, T. F. Jaramillo, J. K. Noskov, J. Rossmeisl, Universality in Oxygen Evolution Electrocatalysis on Oxide Surfaces, *ChemCatChem*. 2011, 3, 1159-1165.